

Secondary amine-activated ferrate(VI) for isoquinoline degradation: Relationship between molecular structure and reactive performance

Original

Secondary amine-activated ferrate(VI) for isoquinoline degradation: Relationship between molecular structure and reactive performance / Wang, Ying; Chen, Liang; Chen, Xin; Bai, Shengchi; Wang, Xiaoqi; Wen, Wen; Liu, Wen; Ma, Jun; Tiraferri, Alberto; Liu, Baicang. - In: JOURNAL OF HAZARDOUS MATERIALS. - ISSN 0304-3894. - 497:(2025). [10.1016/j.jhazmat.2025.139578]

Availability:

This version is available at: 11583/3004346 since: 2025-10-21T17:13:00Z

Publisher:

Elsevier

Published

DOI:10.1016/j.jhazmat.2025.139578

Terms of use:

This article is made available under terms and conditions as specified in the corresponding bibliographic description in the repository

Publisher copyright

Elsevier preprint/submitted version

Preprint (submitted version) of an article published in JOURNAL OF HAZARDOUS MATERIALS © 2025,
<http://doi.org/10.1016/j.jhazmat.2025.139578>

(Article begins on next page)

1 **Secondary Amine-Activated Ferrate(VI): Relationship Between**
2 **Molecular Structure and Reactive Performance**

3
4 Ying Wang ^{a,b}, Liang Chen ^{a,b}, Xin Chen ^{a,b}, Shengchi Bai ^c, Xiaoqi Wang ^c, Wen Wen ^c,
5 Wen Liu ^d, Jun Ma ^e, Alberto Tiraferri ^f, Baicang Liu ^{a,b,*}

6 ^a State Key Laboratory of Hydraulics and Mountain River Engineering, College of
7 Architecture and Environment, Sichuan University, Chengdu, Sichuan, 610207, China

8 ^b Yibin Institute of Industrial Technology, Sichuan University Yibin Park, Section 2,
9 Lingang Ave., Cuiping District, Yibin, Sichuan, 644000, China

10 ^c Research Institute of Petroleum Exploration & Development (RIPE), PetroChina,
11 No. 20 Xueyuan Road Haidian District, Beijing, P. R. China

12 ^d The Key Laboratory of Water and Sediment Sciences, Ministry of Education, College
13 of Environmental Sciences and Engineering, Peking University, Beijing 100871, China

14 ^e State Key Laboratory of Urban Water Resource and Environment, Harbin Institute of
15 Technology, Harbin 150090, China

16 ^f Department of Environment, Land and Infrastructure Engineering, Politecnico di
17 Torino, 10129, Turin, Italy

18 Corresponding author: Baicang Liu, E-mail: bcliu@scu.edu.cn; baicangliu@gmail.com

19 **Abstract**

20 This study systematically elucidates the electronic structure-activity relationship
21 between secondary amines and ferrate (Fe(VI)) activation. Comparative experiments
22 demonstrated that pyrrolidine (Py) significantly outperformed diethylamine (Di) in
23 enhancing Fe(VI)'s oxidation capability across various dosage conditions and pollutant
24 systems, with Py-Fe(VI) achieving approximately 7-fold higher rate constant than
25 Fe(VI) alone for isoquinoline (IQL) degradation, versus a 2-fold improvement observed
26 with the Di-Fe(VI) system. Mechanistic studies combining quenching experiments and
27 EPR characterization corroborated Fe(IV)/Fe(V) as dominant reactive species for IQL
28 degradation, with kinetic modeling revealing that Fe(IV) contributes >80% to IQL
29 degradation in all processes. Electrochemical analyses suggested that Fe(VI) activation
30 by Di and Py might involve the formation of iron-secondary amine complexes. Density
31 functional theory calculations highlighted Py's lower energy barrier for Fe(VI)
32 complexation (27.7 vs. Di's 29.1 kcal/mol), accelerating activation. Secondary amines
33 were shown to stabilize Fe(IV) via coordination, extending its reactive lifetime.
34 Systematic evaluation of various secondary amines revealed a significant negative
35 correlation between the highest occupied molecular orbital energy levels of amines and
36 Fe(VI) activation performance, indicating that moderate electron-donating capacity
37 promotes iron complexation and pollutant degradation. This work establishes a
38 molecular design framework for Fe(VI) activators while providing new insights into
39 high-valent iron-mediated oxidation mechanisms, advancing sustainable water
40 treatment strategies.

41

42 **Keywords**

43 Ferrate; Secondary amines; High-valent iron species; Kinetic model; Theoretical

44 calculations

45

46 **Synopsis**

47 This study established a quantitative correlation mechanism between secondary amine
48 configuration and Fe(VI) activation efficiency.

49

50 **1. Introduction**

51 In recent years, ferrate (Fe(VI)) has attracted extensive research attention as an
52 environmentally friendly and multifunctional water treatment agent due to its unique
53 redox properties ^{1,2}. This compound combines strong oxidizing capacity with
54 multifunctional synergistic effects ³, enabling efficient pathogen inactivation ⁴, organic
55 pollutant degradation ^{5,6}, inorganic pollutant transformation ^{7,8}, and heavy metal ion
56 removal ⁹. Notably, it produces no halogenated disinfection by-products during
57 treatment ¹⁰ and demonstrates superior resistance to water matrix interference compared
58 to chlorine-based disinfectants and ozone ¹¹. Although Fe(VI) demonstrates
59 multifunctional advantages, its practical implementation remains constrained by kinetic
60 limitations in pollutant degradation compared to ozone, Fenton reagents, and other
61 advanced oxidation processes (AOPs) ¹¹. Furthermore, its intrinsic instability poses
62 critical challenges, such as rapid decomposition under acidic conditions ^{12,13}. These pH-
63 dependent limitations collectively restrict its operational versatility across diverse water
64 matrices. To address these bottlenecks, there exists an urgent demand for developing
65 efficient Fe(VI) activation strategies while broadening its operational pH spectrum,
66 thereby enabling more robust and adaptable water treatment applications.

67 Studies have demonstrated that the oxidative capabilities of highly reactive high-
68 valent iron species (Fe(IV)/Fe(V)) markedly surpass those of Fe(VI) ^{1,14}. Existing

69 research confirms that strategies including acid activation ¹⁵, coupling with carbon-
70 based materials ^{2,16}, synergistic oxidation ¹⁷⁻¹⁹, reduction agents ²⁰⁻²³, metal oxide
71 catalysis ²⁴⁻²⁶, and energy field enhancement ^{2,27} can significantly increase the
72 proportion of Fe(IV)/Fe(V) generation in Fe(VI) systems. Of particular interest are
73 amine compounds, which are ubiquitous in natural water systems as reductive media
74 derived from dissolved organic matter and anthropogenic pollutants, such as
75 pharmaceuticals, personal care products, and pesticides ²⁸. Emerging studies have
76 revealed that nitrogen-containing substances like creatinine ²⁹, aliphatic amines ²⁸, and
77 amino acids ¹ can activate Fe(VI) through electron transfer processes, substantially
78 improving pharmaceutical pollutant degradation efficiency. Notably, the amine
79 functional groups in pharmaceuticals play a decisive role in governing their oxidative
80 transformation pathways mediated by Fe(VI). This structural dependence is particularly
81 evident in sulfonamide antibiotics, where the electronic and steric properties of amine
82 moieties dictate the selectivity of oxidation intermediates and final products ³⁰. A
83 critical distinction lies in the activation mechanisms among primary, secondary, and
84 tertiary aliphatic amines: secondary amines exhibit optimal enhancement effects by
85 preferentially generating Fe(IV)-dominated active species, while structurally unique
86 amines, e.g., proline, achieve efficient pollutant removal via Fe(V)-mediated pathways.

87 To systematically elucidate the structure-activity relationship between amine
88 configurations and Fe(VI) activation mechanisms, this study selects diethylamine (Di,
89 [Figure 1a](#)) and pyrrolidine (Py, [Figure 1b](#)) as model compounds. Despite their similar
90 molecular weights and chemical compositions, Di possesses a flexible aliphatic chain
91 structure, whereas Py features a rigid cyclic configuration. This structural difference
92 provides an ideal comparative system for investigating the impact of molecular rigidity
93 on Fe(VI) activation efficiency. The research focuses on four key objectives: (1)

94 comparing the differential enhancement effects of Di and Py on Fe(VI)-mediated
95 degradation of pollutants; (2) identifying critical active species (radical/non-radical)
96 and quantifying their contributions; (3) elucidating molecular mechanisms underlying
97 Fe(VI) activation by different amines; (4) establishing quantitative structure-activity
98 relationships between secondary amine configurations and Fe(VI) activation efficiency
99 to provide guidance for designing high-performance Fe(VI) activators. This work not
100 only advances fundamental understanding of Fe(VI)-amine interactions but also offers
101 scientific foundations for developing ligand-regulated advanced water treatment
102 technologies.

103

104 **2. Materials and Methods**

105 **2.1. Chemicals and Reagents**

106 All the chemicals and reagents used were at least analytical grade; detailed
107 descriptions are provided in the Supporting Information (SI), [Text S1](#). The synthesis
108 procedure for potassium ferrate (Fe(VI)) is presented in [Text S2](#) of the SI

109 **2.2. Experiment Procedures**

110 All batch degradation experiments were conducted at 25 ± 1 °C in glass beakers
111 on a magnetic stirrer (300 rpm). Each pollutant was individually added to the 100 mL
112 system at a concentration of 10 μ M. The reaction was initiated by simultaneously
113 adding the target amount of amine compounds and solid Fe(VI). The pH was
114 maintained at 9.0 ± 0.05 with 10 mM borate buffer. At predetermined time intervals, a
115 1 mL sample was collected and immediately quenched with excess hydroxylamine
116 hydrochloride (100 μ L of 0.1 M $\text{NH}_2\text{OH}\cdot\text{HCl}$), and then filtered (0.22 μ m) into UPLC
117 vials before analysis. Other experiments under different conditions also followed the
118 above procedures. All experiments were performed in at least duplicates and the results

119 are presented as average data with one standard deviation.

120 **2.3. Analytical Methods**

121 The pH values were monitored with a pH meter (FE-28, Mettler Toledo, USA).
122 The measurement of Fe(VI) concentration is detailed in [Text S3](#) Measurements of
123 micropollutant concentrations are described in [Text S4](#) and [Table S1](#). Electron
124 paramagnetic resonance (EPR) analysis is presented in [Text S5](#). Electrochemical tests
125 were conducted in a three-electrode electrochemical cell ([Text S6](#)).

126

127 **2.4. Theoretical calculations**

128 Structure optimizations were carried out with Gaussian 16, Revision A.03 package
129 ³¹ at the B3LYP ^{32,33} level of theory including Grimme's D3 dispersion corrections with
130 Becke-Johnson damping (D3BJ) ^{34,35} with a def2SVP basis set ³⁶⁻³⁹. To identify each
131 stationary point as either an energy minimum or a transition state, analytical frequency
132 calculations were carried out at the same level of theory. On the basis of the gas-phase
133 optimized structures, single point energy values were calculated using the B3LYP
134 functional with a def2-TZVP basis set ³⁶⁻³⁹. All reported energies are based on gas-
135 phase Gibbs free energies for which the electronic energies were corrected to B3LYP
136 with def2-TZVP basis set and solvent effects. The calculation of the Fukui index for Di
137 and Py molecule was performed using the Multiwfn software ⁴⁰ (details shown in [Text](#)
138 [S7](#)).

139 **2.5. Kinetic Modeling**

140 The program Kintecus V6.51 (www.kintecus.com) was used for kinetic fitting and
141 simulation for IQL oxidation in the Fe(VI) alone, Di-Fe(VI), and Py-Fe(VI) systems.
142 The reaction equations employed in the kinetic model are displayed in [Tables S2-S4](#),
143 and the models were validated by the model sensitivity analysis ([Texts S8-S10](#) and

144 [Figures S10–S19](#))⁴¹.

145

146 **3. Results and Discussion**

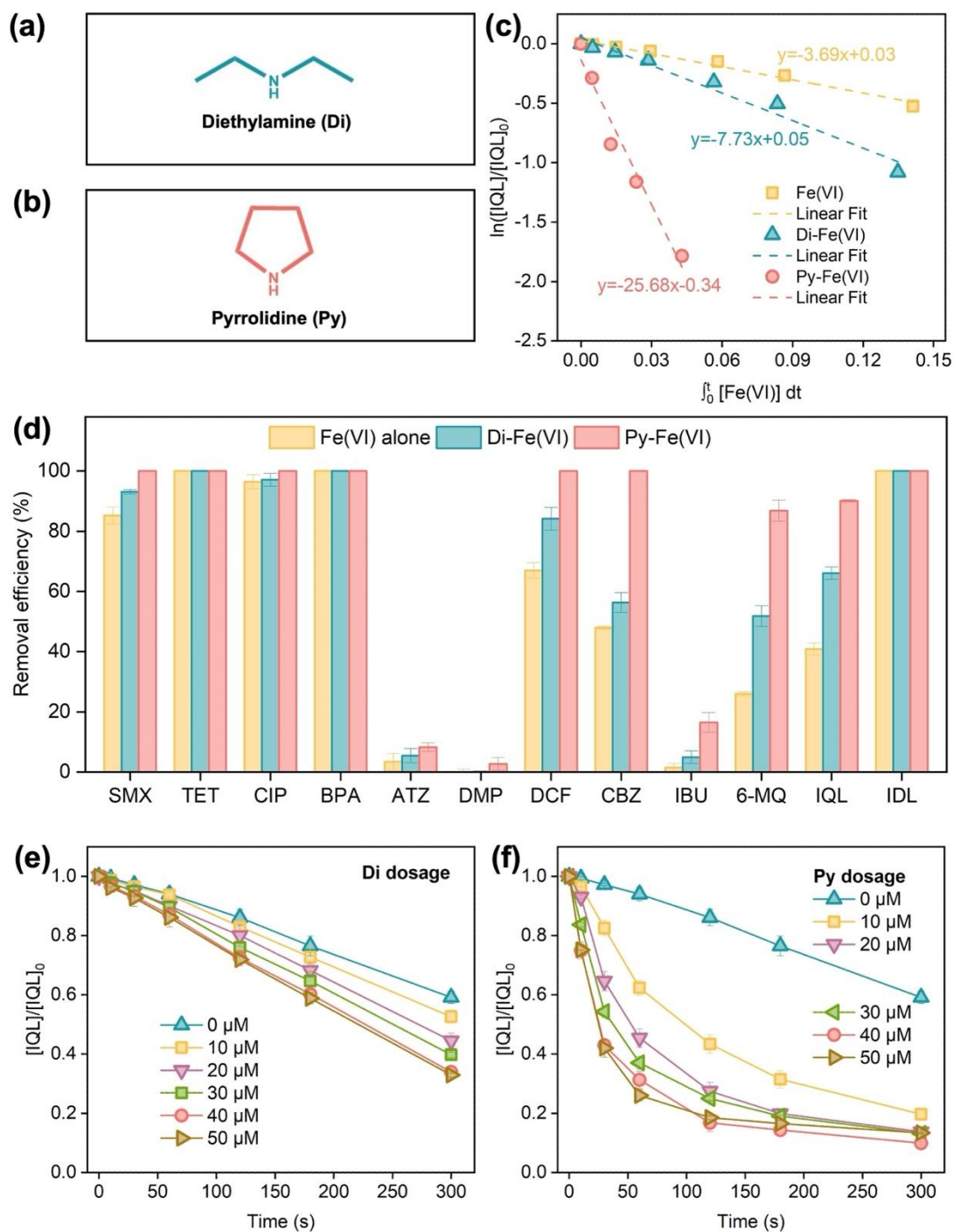
147 **3.1. Oxidation Performance of secondary amine-Fe(VI)**

148 The degradation of isoquinoline (IQL) by individual systems (Di alone, Py alone,
149 Fe(VI) alone) and combined systems (Di-Fe(VI), Py-Fe(VI)) was systematically
150 investigated. As shown in [Figure S1](#), neither Di nor Py alone exhibited any IQL
151 degradation capability within 300 seconds of reaction. In contrast, the Fe(VI) alone, Di-
152 Fe(VI), and Py-Fe(VI) systems achieved IQL removal efficiencies of 40.9%, 66.1%,
153 and 90.1%, respectively. As depicted in [Figure 1c](#), all the three processes followed
154 second-order kinetics. The rate constants for Di-Fe(VI) and Py-Fe(VI) were determined
155 to be $7.73 \text{ M}^{-1}\text{s}^{-1}$ and $25.7 \text{ M}^{-1}\text{s}^{-1}$, respectively, representing approximately 2-fold and
156 7-fold enhancements compared to the sole Fe(VI) process ($3.69 \text{ M}^{-1}\text{s}^{-1}$). It is obvious
157 that the introduction of Di or Py significantly enhanced the Fe(VI)-mediated
158 degradation of IQL.

159 Additionally, the degradation of 12 micropollutants were systematically evaluated
160 with Di alone, Py alone, Fe(VI) alone, Di-Fe(VI), and Py-Fe(VI) processes. The target
161 contaminants included: antibiotics, i.e., sulfamethoxazole (SMX), tetracycline (TET),
162 ciprofloxacin (CIP); endocrine disruptors, i.e., bisphenol A (BPA, atrazine (ATZ),
163 dimethyl phthalate (DMP); pharmaceuticals, i.e., diclofenac (DCF), carbamazepine
164 (CBZ), ibuprofen (IBU); representative organics in shale gas wastewater, i.e., IQL, 6-
165 Methylquinoline (6-MQ), indoline (IDL) (see [Figure S2](#) and [Figure 1d](#)). Within 300 s,
166 Di and Py alone exhibited negligible degradation for all tested micropollutants. Fe(VI)
167 achieved partial degradation of 9 out of 12 contaminants within 5 minutes, with the
168 exceptions of DMP, IBU, and ATZ, likely because Fe(VI) typically exhibits high

169 reactivity toward electron-rich contaminants but inertness toward electron-deficient
170 ones ²⁷. Notably, except for DMP, TET, BPA, and IDL, the latter three having already
171 achieved 100% degradation by Fe(VI) alone, the addition of Di and Py enhanced the
172 degradation of all tested micropollutants. Py consistently exhibited a stronger catalytic
173 enhancement than Di, with this phenomenon observed across different pollutant
174 categories, implying the broad applicability of the observed catalytic behavior.

175 The dosage-dependent effects of secondary amines on IQL degradation were
176 evaluated in Di-Fe(VI) and Py-Fe(VI) processes. As shown in [Figures 1e–f](#), increasing
177 the Di or Py concentrations from 10 to 40 μM initially enhanced IQL degradation
178 efficiency, followed by a slight decline at 50 μM . This phenomenon likely arised from
179 excessive Di or Py reducing high-valent iron species (Fe(VI)/Fe(V)/Fe(IV)) to less
180 reactive lower-valence states (Fe(III)/Fe(II)), which commonly exhibit diminished
181 oxidative capacity for IQL degradation. Notably, Py exhibited persistent catalytic
182 superiority over Di across all tested dosages under identical experimental conditions,
183 thereby emphasizing the reproducibility and mechanistic stability of this enhancement
184 phenomenon. Investigations into additional influencing parameters (e.g., pH,
185 coexisting ions) are provided in [Figures S3–S4](#) and [Text S11–S12](#).



186

187 **Figure 1.** Structural formula of Di (a) and Py (b); Degradation kinetics of IQL by Fe(VI),

188 Di-Fe(VI), and Py-Fe(VI) processes (c); Removal of various pollutants by Fe(VI) alone,

189 Di-Fe(VI), and Py-Fe(VI) processes (d); Effect of Di dosage (e) and Py dosage (f) on

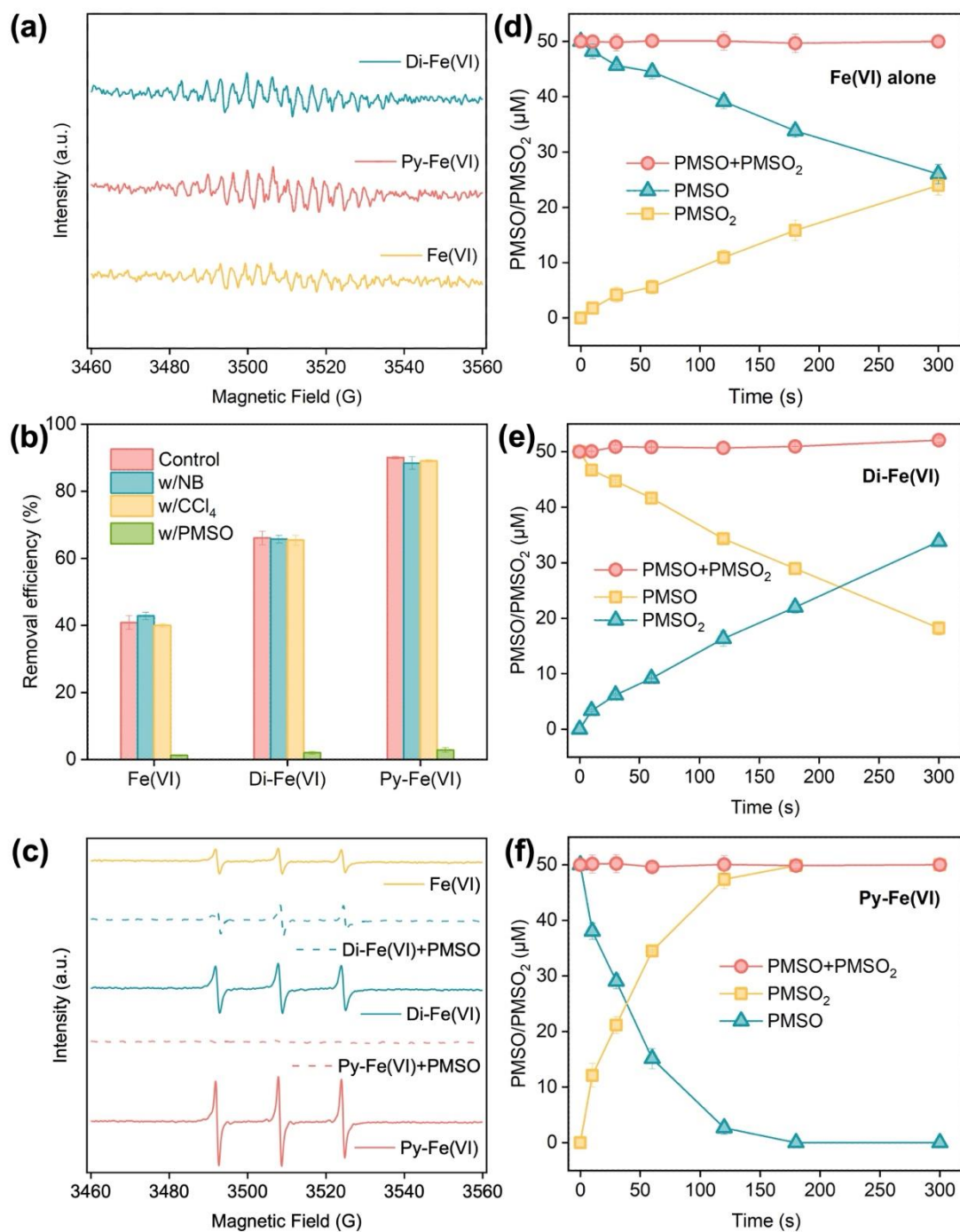
190 IQL removal. Experiment conditions: pH = 9.0, $[IQL]_0 = 10 \mu$ M, $[Di]_0 = [Py]_0 = 40 \mu$ M,

191 $[Fe(VI)]_0 = 500 \mu$ M.

192

193 3.2. Evidence for the Fe(V)/Fe(IV) Contribution

194 To examine the possible reactive oxygen species (ROS, e.g., HO[•], O₂^{•-}, and ¹O₂)
195 and reactive iron species (Fe(IV)/Fe(V)) for IQL depletion during the Fe(VI)-based
196 processes, a combination of EPR spectroscopy, quenching tests, and probe compounds
197 was utilized (Text S13). As depicted in Figure 2a, HO[•] was likely not involved in any
198 of the processes, since no signal of the DMPO-HO[•] adduct was observed. The role of
199 HO[•] was also ruled out using the probe compound nitrobenzene (NB)^{42,43}, as NB had
200 no effect on the removal of IQL (Figure 2b), and no removal of NB was observed in
201 these systems (Figure S5). Then, to identify the role of O₂^{•-}, CCl₄ was chosen as a
202 scavenger for O₂^{•-}, since CCl₄ is relatively reactive with O₂^{•-} ($1.1 \times 10^9 \text{ M}^{-1} \text{ s}^{-1}$)^{44,45}.
203 The presence of 50 mM CCl₄ showed a negligible inhibition on the abatement of IQL,
204 indicating that O₂^{•-} did not have substantial involvement in any of the systems, with or
205 without secondary amines (Figure 2b and Figure S6). The employment of nitro blue
206 tetrazolium (NBT) as a characteristic probe also ruled out the role of O₂^{•-}, because the
207 absorbance of NBT could not be reduced (Figure S7) and there was no characteristic
208 absorption peak of NBT-O₂^{•-} at 560 nm⁴⁶ (Figure S8). Furthermore, visible light-rose
209 bengal (Vis-RB) process, a classical system that only produces ¹O₂⁴⁷, was conducted
210 to verify the role of ¹O₂. As summarized in Figure S9, the Vis-RB process did not lead
211 to the degradation of IQL, reflecting that the ¹O₂ was not responsible for IQL
212 elimination. Although a TEMP-¹O₂ signal was observed (Figure 2c), it may not be
213 attributed to ¹O₂, a mechanism that will be discussed below. The results collectively
214 excluded the significant roles of ROS in IQL removal. In other words, active iron
215 species oxidation should be the largely main mechanism responsible for removing IQL
216 within the Fe(VI), Di-Fe(VI), and Py-Fe(VI) systems.



217

218 **Figure 2.** EPR spectra of DMPO-HO' in various processes (a); Influence of different
 219 scavengers and probes on the removal of IQL by Fe(VI) alone, Di-Fe(VI), and Py-Fe(VI)
 220 processes (b); EPR spectra of TEMP-¹O₂ in various processes (c); Degradation of
 221 PMSO and generation of PMSO₂ in Fe(VI) alone (d), Di-Fe(VI) (e), and Py-Fe(VI) (f)
 222 processes. Experiment conditions: pH = 9.0, [IQL]₀ = 10 μM, [Di]₀ = [Py]₀ = 40 μM,
 223 [Fe(VI)]₀ = 500 μM, [PMSO]₀ = 1 mM, [NB]₀ = 10 μM, [CCl₄]₀ = 50 mM.

224 It is well known that methyl phenyl sulfoxide (PMSO) can be oxidized by high-
225 valent iron (Fe(IV)/Fe(V)) into PMSO₂ through oxygen-atom transfer pathway, which
226 observably differs from the radical-based oxidation pathway, during which PMSO
227 mainly transforms into other products, such as hydrolyzed PMSO^{16,48}. Typically,
228 Fe(IV)/Fe(V) exhibits higher oxidation capability than Fe(VI) with PMSO. Thus,
229 PMSO has been frequently used to check the formation of Fe(IV)/Fe(V) in Fe(VI)-
230 based oxidation processes. When 1 mM of PMSO was added into Fe(VI), Di-Fe(VI),
231 and Py-Fe(VI) systems, the removal performance of IQL was remarkably restrained
232 (Figures 2b). For instance, when 1 mM PMSO was added to the reaction solution, only
233 1.24%, 2.03%, and 2.84% of IQL abatement was obtained after 300s treatment for
234 Fe(VI) alone, Di-Fe(VI), and Py-Fe(VI), respectively, while 40.9%, 66.1%, and 90.1%
235 IQL removal was achieved by the corresponding three processes in the absence of
236 PMSO. The obvious suppression phenomenon of IQL degradation may be attributed to
237 PMSO and IQL competing for Fe(IV)/Fe(V). This also suggested that Fe(IV)/Fe(V)
238 played a dominant role in IQL removal.

239 Furthermore, the degradation of PMSO by sole Fe(VI), Di-Fe(VI), and Py-Fe(VI)
240 processes was explored. As reflected in Figures 2d–2f, the proportion of generated
241 PMSO₂ to degraded PMSO consistently remained around 100% throughout the entire
242 reaction sequence, demonstrating that nearly all PMSO degradation was converted into
243 PMSO₂ through the oxygen transfer mechanism in all processes. The findings
244 additionally confirm that the involvement of radicals may be considered negligible,
245 with Fe(V) and Fe(IV) being identified as the key reactive species responsible for the
246 removal of IQL. Importantly, compared with sole Fe(VI) process, Di-Fe(VI) and Py-
247 Fe(VI) processes achieved faster degradation of PMSO and formation of PMSO₂,
248 which is attributed to the addition of Di and Py speeding up the generation of

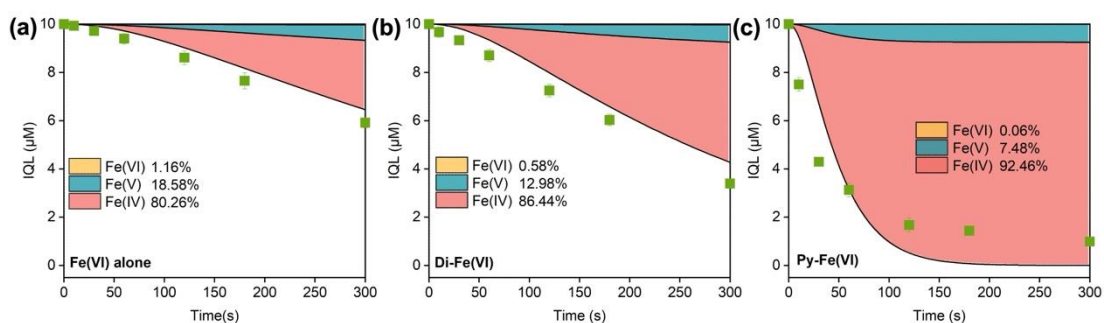
249 Fe(IV)/Fe(V). [Figure 2c](#) presents the EPR spectrum of TEMP-¹O₂ in various processes:
250 a signal for the TEMP-¹O₂ adduct was observed in the Fe(VI) alone process, while the
251 signals for adduct in the Di-Fe(VI) and Py-Fe(VI) systems were significantly stronger
252 than that of the Fe(VI) alone. Previous research has reported that high-valent iron
253 (Fe(IV), Fe(V), Fe(VI)) could lead to false positives in ¹O₂ EPR detection⁴⁹. Therefore,
254 the signals here were likely attributed to high-valent iron, since with the presence of
255 PMSO the signals were significantly reduced. The enhanced signal in Di-Fe(VI) and
256 Py-Fe(VI) process also indicated that the production of Fe(IV)/Fe(V) was increased. In
257 summary, Fe(V)/Fe(IV) was likely the dominant reactive species for IQL removal in
258 the Di-Fe(VI) and Py-Fe(VI) reaction processes.

259

260 **3.3. Identification of Fe(IV)/Fe(V)/Fe(VI) Contribution to IQL degradation**

261 The results discussed above corroborate that only Fe(IV), Fe(V), and Fe(VI) were
262 involved in IQL oxidation. However, the specific contributions of ferrates in this
263 process are still unknown. Thus, a model was built based on major reactions (details in
264 [Tables S2–S4](#)) and employed to fit the kinetics of IQL degradation by Kintecus software.
265 Based on the modeled results, Fe(V) and Fe(IV) contributed 18.6% and 80.3% to IQL
266 oxidation in the Fe(VI) alone process, respectively. Fe(IV) was the dominant reactive
267 species for IQL degradation in the Di-Fe(VI) process (86.4% contribution), while the
268 contribution of Fe(V) was 12.9%. Similarly, Fe(IV) accounted for 92.5% of the IQL
269 oxidation in the Py-Fe(VI) process, whereas Fe(V) contributed only 7.48% to IQL
270 oxidation. Of note is that the contribution of Fe(IV) obviously increased in the Di-Fe(VI)
271 and Py- Fe(VI) processes, in comparison with that of the sole Fe(VI) system ([Figures](#)
272 [3](#)), suggesting the role of Fe(IV). The above models were tested with a sensitivity
273 analysis and model validation ([Figures S10–S18](#)) and the results confirmed that the

274 fitting results were valid. Furthermore, the concentration profiles of ferrates in Fe(VI)
 275 alone, Di-Fe(VI), and Py-Fe(VI) were also determined based on the simulation. [Figure](#)
 276 [S19](#) shows that the concentration of Fe(IV) was about three orders of magnitude higher
 277 than that of Fe(V) during IQL degradation by three different processes. Note that the
 278 concentration of Fe(IV) in the Di-Fe(VI) and Py-Fe(VI) processes were increased
 279 compared with the case of Fe(VI) alone, suggesting the increased amounts of reactive
 280 species under the activation of Di and Py. In general, the results strongly suggest that
 281 Fe(IV) played a dominant role in all the three processes.



282

283 **Figure 3.** Contributions of Fe(IV), Fe(V), and Fe(VI) to IQL degradation by Fe(VI)
 284 alone (a), Di-Fe(VI) (b), and Py-Fe(VI) (c) processes.. Experiment conditions: pH =
 285 9.0, $[IQL]_0 = 10 \mu\text{M}$, $[Di]_0 = [Py]_0 = 40 \mu\text{M}$, $[Fe(VI)]_0 = 500 \mu\text{M}$.

286

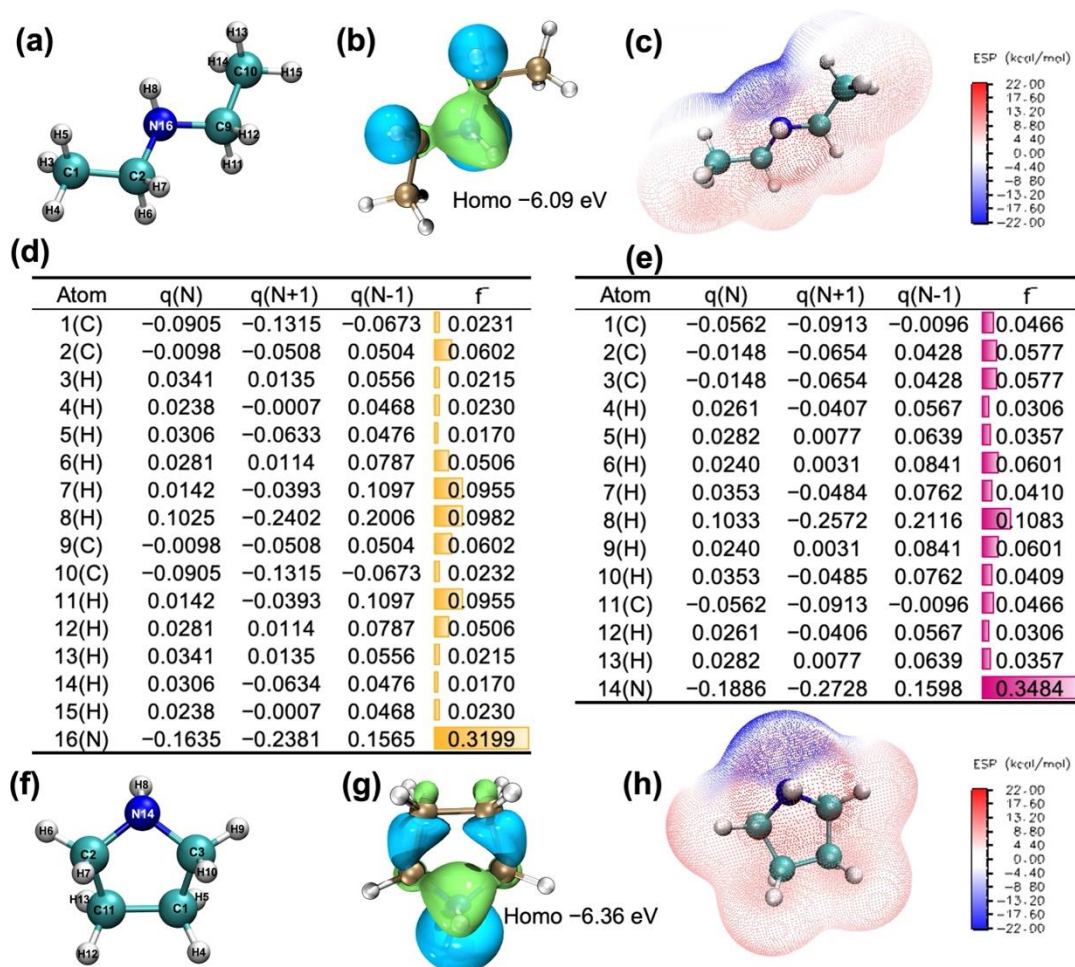
287 3.4. Activation Mechanism of Fe(VI) by Secondary Amines and Corresponding 288 Theoretical Calculations

289 As mentioned above, both Di and Py enhanced the oxidative performance likely
 290 by activating Fe(VI) to generate Fe(IV)/Fe(V) intermediates. In this process, Fe(VI)
 291 acts as an electron acceptor, while Di and Py serve as electron donors. This section will
 292 delve into the specific activation sites of Fe(VI) by Di and Py, along with the relevant
 293 functional groups, through DFT calculations. [Figure 4a](#), [4c](#), [4f](#), and [4h](#) illustrates the

294 distribution of negative and positive electrostatic potentials around Di and Py using a
295 gradient from blue to red. The deep blue regions represent areas of concentrated
296 negative charge, surrounding N atoms, which correlate with stronger affinity for high-
297 valent Fe active species and greater potential for chemical activation. By analyzing the
298 electron density isosurface maps of f^- , f^+ , and f^0 on the surfaces of Di and Py, it is
299 evident that the -NH groups in Di and Py are expected to exhibit higher reactivity
300 (Figure S20). While the isosurface mapping of electron density provides intuitive
301 insights, it does not facilitate detailed quantitative analysis of Fukui function values. To
302 enable a more streamlined and intuitive interpretation, a simplified version of the Fukui
303 function was employed to predict the sites in Di and Py molecules that are susceptible
304 to attack by reactive species. The condensed Fukui function theory indicates that larger
305 f^- , f^+ , and f^0 values correspond to atoms more prone to electrophilic, nucleophilic, and
306 radical attacks, respectively. The 3N site in Di and the 1N site in Py display the highest
307 f^- values (Figure 4d–4e), suggesting these locations are likely the first to be targeted by
308 Fe(VI).

309 The highest occupied molecular orbital (HOMO) is a critical indicator reflecting
310 the electron-donating capacity of a molecule. Figure 4b and 4g reveals that the HOMOs
311 of both Di and Py were apt to be localized on the -NH groups. Thus, the electrons in the
312 -NH groups of Di and Py are readily delocalized. The HOMO value of Py (-6.36 eV)
313 is more negative than that of Di (-6.09 eV), indicating that Di has superior electron-
314 donating capability to Fe(VI) compared to Py. This observation, which exhibits an
315 inverse correlation with the degradation trend of IQL, will be analyzed in subsequent

316 sections.



317

318 **Figure 4.** Chemical structure of Di (a) and Py (f); Highest occupied molecular orbital
 319 (HOMO) of Di (b) and Py (g); Electrostatic potential (ESP) distribution of Di (c) and
 320 Py (h); Natural population analysis (NPA) charge distributions and condensed Fukui
 321 index (f^-) of Di (d) and Py (e).

322

323 3.5. Coordination between Fe(VI) and Secondary Amines

324 In-situ electrochemical analysis was further used to investigate the promoting
 325 mechanism of Di-Fe(VI) and Py-Fe(VI) processes. [Figure 5a](#) shows the variation curve
 326 of the open circuit potential with time, using a mercury oxide electrode (HgO) as the

327 reference electrode and Pt sheet electrodes as the working and counter electrodes. After
328 Fe(VI) was added to the solution, the potential rose immediately from initial 0.68 V to
329 final 0.83 V after stabilization. Because Fe(VI) is a strong oxidizing agent, the addition
330 of Fe(VI) enhanced the oxidizing power, resulting in a higher potential. After the
331 subsequent addition of Di or Py, the potential began to decrease, indicating that Di and
332 Py acted as reductants in the reaction, donating electrons and reducing Fe(VI) to low-
333 valent forms, such as Fe(IV) and Fe(V). Next, the residual Fe(VI) concentrations for
334 Fe(VI) alone, Di-Fe(VI), and Py-Fe(VI) processes were investigated (Figure 5b). After
335 300 s reaction time, the value of $[\text{Fe(VI)}]/[\text{Fe(VI)}]_0$ ratio was 0.94, 0.90, and 0.58 in the
336 sole Fe(VI), Di-Fe(VI), and Py-Fe(VI) systems, respectively, indicating that the
337 consumption of Fe(VI) could be remarkably improved with the presence of Di and Py.
338 The consumption of Fe(VI) was effectively improved by Di and Py, while the Di-Fe(VI)
339 and Py-Fe(VI) processes still showed higher performance for IQL abatement than sole
340 Fe(VI). As a whole, these results indicate that more reactive species, such as active
341 high-valent iron intermediate species, (Fe(IV), Fe(V)), may be formed by the
342 combination of Di and Py with Fe (VI) ^{14,28}.

343 Cyclic voltammetry (CV) measurements were conducted for the three systems
344 (Figure 5c). Redox peaks were observed in all three systems; given the limited
345 electrochemical data for Fe(VI) in the existing literature, it is hypothesized that the
346 observed reduction may correspond to the reductive conversion of high-valent Fe
347 species to low-valent forms, such as Fe(IV) and Fe(V). The Py-Fe(VI) process exhibited
348 the highest peak current, indicating the presence of more active iron species in the
349 process. It is noteworthy that, compared to the Fe(VI) alone, both the Di-Fe(VI) and
350 Py-Fe(VI) processes exhibited a positive shift in oxidation peaks and a negative shift in
351 reduction peaks in their CV curves. This phenomenon could be attributed to the

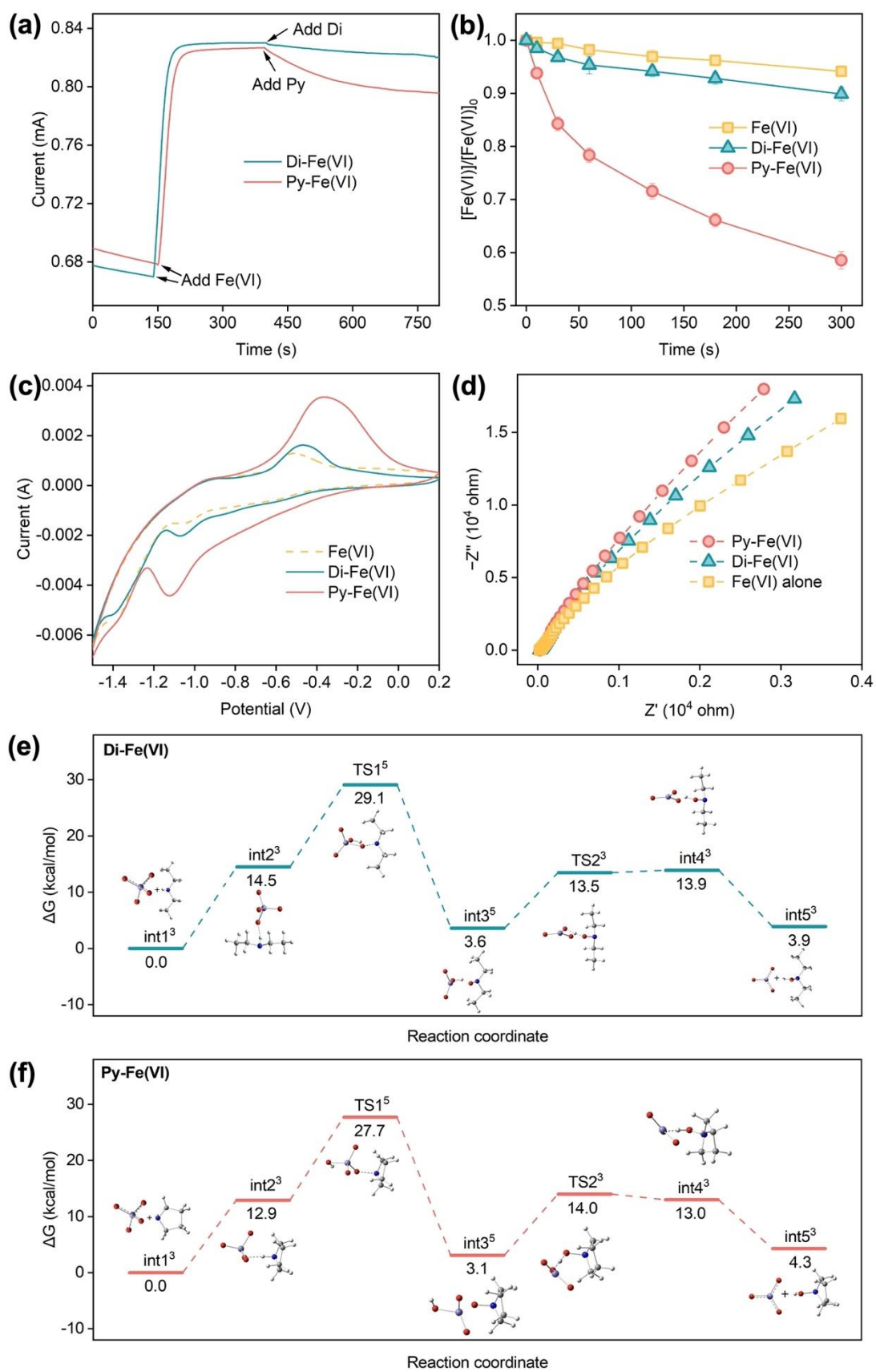
352 coordination of Di and Py with Fe(VI) to form complexes, where the complexation
353 altered the redox potential of Fe(VI). The negative shift in reduction peaks indicates
354 that the Fe(VI) complexes are more easily reduced than free Fe(VI), suggesting a
355 lowering of their reduction energy barrier. Furthermore, electrochemical impedance
356 spectroscopy (EIS) was employed to evaluate the charge transfer resistance of the
357 catalysts during redox reactions ⁵⁰ (Figure 5d). A lower Tafel slope indicates higher
358 intrinsic activity and reduced transport limitations ⁵¹. The order of the semicircle radii
359 in the Nyquist plots was: Fe(VI) < Di-Fe(VI) < Py-Fe(VI), with Py-Fe(VI) process
360 showing the largest radius. This phenomenon is due to the coverage of the electrode
361 surface by the complexes after their formation, leading to an increase in resistance.
362 These results validate the hypothesis discussed above: taken together, the efficacy of Di
363 and Py in activating Fe(VI) for IQL removal appears to be influenced by their
364 coordination properties.

365 To elucidate the superior activation performance of Py over Di in enhancing
366 Fe(VI)-mediated IQL degradation and unravel the mechanistic origins of differential
367 Fe(V)/Fe(IV) contribution ratios, we conducted density functional theory (DFT)
368 calculations to compare the reaction energy barriers of the various systems.
369 Thermodynamic parameters for reactants, transition states (TS), intermediates, and
370 products in Di- and Py-Fe(VI) reaction systems are summarized in Tables S7–S9, with
371 Gibbs free energies illustrated in Figures 5e and 5f. The results indicate that the
372 activation energy barrier for Py to form transition state TS1 with Fe(VI) (27.7 kcal/mol)
373 is lower than that of Di (29.1 kcal/mol), implying faster reaction kinetics for Py. This
374 observation aligns with the enhancement trend discussed in Section 3.1, which
375 suggested that Py-Fe(VI) exhibited superior IQL degradation compared to Di-Fe(VI).
376 This phenomenon may arise from the conformational rigidity of Py's cyclic structure,

377 which facilitates optimal geometric alignment for hydrogen abstraction and oxygen
378 transfer processes. Concurrently, intracyclic orbital conjugation and favorable lone-pair
379 electron orientation within the pyrrolidine ring may synergistically promote Fe-O bond
380 cleavage while stabilizing O-N bond formation. Although Di is characterized by a
381 marginally lower TS2 barrier (13.5 vs. 14.0 kcal/mol for Py), the decisive TS1 disparity
382 may govern the overall reaction kinetics, establishing Py's superiority.

383 Furthermore, we note that the energy barrier for the formation of complex int2
384 between Py and Fe(VI) (12.9 kcal/mol) was found to be lower than the corresponding
385 value for Di (14.5 kcal/mol), indicating that Py should coordinate more efficiently with
386 Fe(VI). During the reaction between Py and Fe(VI), the energy barrier for the formation
387 of complex int4 between Fe(IV) and Py(O) (13.0 kcal/mol) was also found to be lower
388 than the corresponding value for Di (13.9 kcal/mol), suggesting that the Fe(IV)-Py(O)
389 complex should be more stable and may effectively inhibit its conversion into less
390 reactive Fe(II)/Fe(III). Based on [Tables S2–S4](#), Fe(V) in all three systems is primarily
391 generated from the reaction between Fe(VI) and Fe(II). Consequently, the Fe(IV)
392 contribution in the Py-Fe(VI) system is higher than that in the Di-Fe(VI) system, while
393 the Fe(V) contribution is lower. Overall, Py may provide superior advantages in
394 intermediate formation and stabilization, further supporting its kinetic dominance.

395 In summary, the findings discussed here suggest that the enhanced pollutant
396 degradation performance of secondary amines (e.g., Di, Py) with Fe(VI) is closely
397 related to their ability to form stable complexes with high-valent iron species
398 (Fe(VI)/Fe(IV)/Fe(V)). Notably, differences in coordination capacity are hypothesized
399 to directly determine the superiority or inferiority of the resulting catalytic performance.



400

401 **Figure 5.** Change of open-circuit potential in Di-Fe(VI) and Py-Fe(VI) processes (a);

402 Decomposition of Fe(VI) in reaction solution with or without Di and Py (b); Cycle
403 voltammetry measurements of Fe(VI), Di-Fe(VI), and Py-Fe(VI) processes (c); EIS
404 measurements of Fe(VI), Di-Fe(VI), and Py-Fe(VI) processes (d); Gibbs free energy
405 pathway between Di and Fe(VI) (e), Py and Fe(VI) (f). Experiment conditions: pH =
406 9.0, [IQL]₀ = 10 μM, [Di]₀ = [Py]₀ = 40 μM, [Fe(VI)]₀ = 500 μM.

407

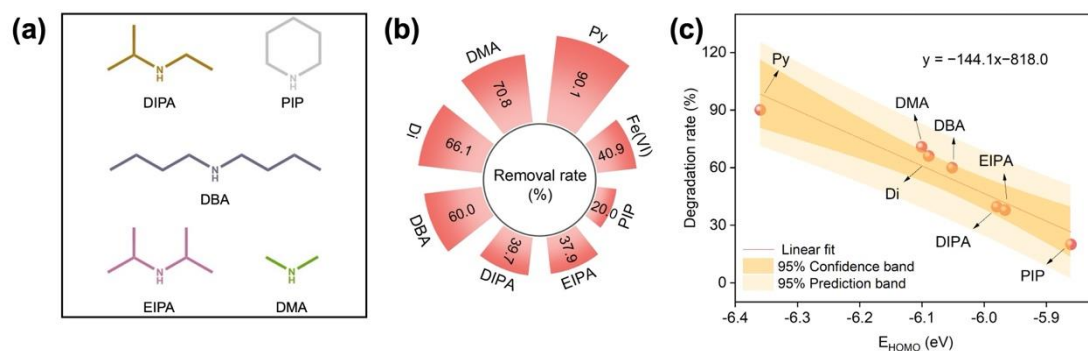
408 **3.6. Structure Effects of Secondary Amine**

409 The regulatory effects of seven structurally distinct secondary amines was
410 investigated in the Fe(VI)-mediated degradation of isoquinoline (IQL). The tested
411 amines included five linear secondary amines: dimethylamine (DMA), Di,
412 dibutylamine (DBA), diisopropylamine (DIPA), and N-ethylisopropylamine (EIPA),
413 along with two cyclic secondary amines, namely, Py and piperidine (PIP). Among the
414 linear amines, DMA, Di, and DBA possess straight-chain alkyl groups, whereas DIPA
415 and EIPA feature branched structures (Figure 6a). Results indicated that DMA, Di, DBA,
416 and Py enhanced Fe(VI)- mediated IQL degradation, with efficacy following the order:
417 Py > DMA > Di > DBA (Figure 6b). Notably, the cyclic amine Py exhibited superior
418 activation performance compared to linear amines, likely attributed to its rigid
419 molecular structure facilitating stable complexation with Fe(VI). Such coordination
420 may effectively stabilize reactive iron intermediates. In linear amine systems,
421 shortening the alkyl chain length improved activation efficiency, highlighting the
422 critical role of steric hindrance, with longer chains hindering optimal coordination.
423 However, DIPA, EIPA, and PIP inhibited degradation. This anomaly may arise from
424 unique steric effects imposed by their branched structures or electronic interference
425 with Fe(VI) redox processes.

426 Although preliminary comparisons between Di and Py showed a positive

427 correlation trend between their coordination ability with Fe(VI) and IQL removal
428 efficiency, directly quantifying the coordination capabilities of various secondary
429 amines with Fe(VI) faces significant challenges. Coordination strength is influenced by
430 multiple factors, including solvent effects, steric hindrance, and dynamic reaction
431 conditions, which complicate precise measurement or quantitative estimation.⁵² In
432 contrast, the HOMO energy levels (E_{HOMO}) calculated via quantum chemical methods
433 should offer a stable theoretical measure of the intrinsic electron-donating properties of
434 amines. Moreover, as discussed in Sections 3.4 and 3.5, there appears to be a theoretical
435 relationship between E_{HOMO} and coordination ability: higher E_{HOMO} values were
436 associated with weaker coordination. Based on this premise, we investigated the
437 correlation between IQL removal and E_{HOMO} values for seven secondary amines.
438 Quantum chemical calculations revealed a significant negative correlation between IQL
439 degradation and the E_{HOMO} levels (Figure 6c, Figure S21). This finding suggests that
440 the electron-donating capacity of secondary amines inversely correlates with their
441 coordination ability. Effective Fe(VI) activation requires moderate electron-donating
442 capacity: excessive electron donation (high HOMO levels) may trigger over-reduction
443 of Fe(VI) to Fe(II)/Fe(III), prematurely depleting its oxidative potential.

444 In summary, this study suggests that the electron-donating capacity of secondary
445 amines exhibits a negative correlation with Fe(VI) activation, thus providing theoretical
446 guidance for designing high-performance Fe(VI) activators, while also unveiling the
447 intricate relationships between ligand electronic properties and oxidant activation
448 mechanisms.



449

450 **Figure 6.** Chemical structure of DIPA, PIP, DBA, EIPA, and DMA (a); Degradation
 451 efficiencies of IQL by Fe(VI) with and without secondary amines (b); Correlation
 452 between the HOMO energy levels (E_{HOMO}) and IQL degradation rate (c); HOMO and
 453 LUMO of Py, Di, DIPA, PIP, DBA, EIPA, and DMA (d). Experiment conditions: pH =
 454 9.0, $[\text{IQL}]_0 = 10 \mu\text{M}$, $[\text{secondary amines}]_0 = 40 \mu\text{M}$, $[\text{Fe(VI)}]_0 = 500 \mu\text{M}$.

455

456 4. Environmental Implications

457 This study discusses the critical role of secondary amines in enhancing Fe(VI)-
 458 based oxidation systems. By identifying Di and Py as high-performance activators
 459 (degradation kinetics accelerated by ~2-fold and 7-fold compared to Fe(VI) alone,
 460 respectively), the findings should enable reductions in Fe(VI) dosage and treatment
 461 time, thereby minimizing secondary sludge generation and chemical costs. The
 462 dominance of Fe(IV) over free radicals in pollutant degradation further reduces risks of
 463 toxic byproduct formation (e.g., halogenated organic compounds), aligning with safer
 464 water purification strategies. Importantly, the revealed negative correlation between the
 465 HOMO energy levels of secondary amines and their activation efficiency provides a
 466 molecular blueprint for designing eco-friendly amine ligands, guiding synthetic
 467 chemistry toward non-toxic, electronically tunable alternatives. The iron-amine
 468 complexation mechanism may also inspire low-carbon solutions that could convert
 469 nitrogen-containing waste compounds into Fe(VI) activators. Furthermore, the amine-

470 coordination-mediated extension of Fe(IV) lifetime enhances pollutant mineralization
471 efficiency, which is crucial for eliminating persistent micropollutants in aquatic
472 environments.

473 It should be emphasized that due to the structural complexity of secondary amines,
474 the impacts and underlying mechanisms of Fe(VI)-mediated pollutant degradation by
475 secondary amines containing additional functional groups (e.g., -COOH, -OH) remain
476 unclear. Further investigations into the fundamental mechanisms of introducing other
477 functional groups into Fe(VI)-based pollutant oxidation systems are essential. Such
478 studies will deepen the understanding of secondary amine-Fe(VI) interactions and
479 strengthen the theoretical foundation for designing highly efficient secondary amine-
480 based compounds to activate Fe(VI).

481

482 **Acknowledgments**

483 This work was supported by the National Natural Science Foundation of China
484 (52070134, 52270075), Outstanding Youth Science Foundation of Sichuan Province
485 Natural Science Foundation (2025NSFJQ0010), Litree Purifying Technology Co., Ltd.
486 Project (2021H012). A.T. acknowledges the support of Politecnico di Torino. We would
487 like to thank the Institute of New Energy and Low-Carbon Technology, Sichuan
488 University, for Raman tests. We would like to thank the Analytical & Testing Center of
489 Sichuan University for EPR measurement.

490 **References**

- 491 (1) Rougé, V.; Nguyen, P. T. T. H.; Allard, S.; Lee, Y. Reaction of Amino Acids with
492 Ferrate(VI): Impact of the Carboxylic Group on the Primary Amine Oxidation
493 Kinetics and Mechanism. *Environ. Sci. Technol.* **2023**, *57* (47), 18509–18518.
494 <https://doi.org/10.1021/acs.est.2c03319>.
- 495 (2) Deng, Z. K.; Zhu, J. Y.; Zeng, C. Y.; Mu, R.; Ma, Y. F.; Zhang, Z. L. Highly
496 Efficient Activation of Ferrate (VI) via Corncob Biochar Assisted by
497 Electrochemistry for the Removal of Sulfamethoxazole from Water. *Chem. Eng.*
498 *J.* **2024**, *484*, 149479. <https://doi.org/10.1016/j.cej.2024.149479>.
- 499 (3) Sharma, V. K.; Kazama, F.; Jiangyong, H.; Ray, A. K. Ferrates (Iron(VI) and
500 Iron(V)): Environmentally Friendly Oxidants and Disinfectants. *J. Water Health*
501 **2005**, *3* (1), 45–58. <https://doi.org/10.2166/wh.2005.0005>.
- 502 (4) Mao, Y.; Chen, Z.; Lu, Y.; Cao, K. F.; Wu, Y. H.; Hu, H. Y. Inactivation of Bacteria
503 in Water by Ferrate(VI): Efficiency and Mechanisms. *Environ. Sci. Technol.* **2023**,
504 *57* (49), 20893–20904. <https://doi.org/10.1021/acs.est.3c05118>.
- 505 (5) Qi, X. C.; Ding, L. Z.; Jian, C. Q.; Liu, R. T.; Liu, N.; Qu, D. Ferrate(VI) Oxidation
506 of Substituted Nitrobenzene Compounds: Kinetics, Degradation, and Oxidized
507 Products. *Chem. Eng. J.* **2024**, *488*, 150921.
508 <https://doi.org/10.1016/j.cej.2024.150921>.
- 509 (6) Sharma, V. K.; Wang, J.; Feng, M.; Huang, C.-H. Oxidation of Pharmaceuticals
510 by Ferrate(VI)–Amino Acid Systems: Enhancement by Proline. *J. Phys. Chem. A*
511 **2023**, *127* (10), 2314–2321. <https://doi.org/10.1021/acs.jpca.3c00134>.

- 512 (7) Yates, B. J.; Zboril, R.; Sharma, V. K. Engineering Aspects of Ferrate in Water and
513 Wastewater Treatment – a Review. *J. Environ. Sci. Health Part a* **2014**, *49* (14),
514 1603–1614. <https://doi.org/10.1080/10934529.2014.950924>.
- 515 (8) Tiwari, D. Ferrate(VI) a Greener Solution: Synthesis, Characterization, and
516 Multifunctional Use in Treating Metal-Complexed Species in Aqueous Solution.
517 In *Ferrites and Ferrates: Chemistry and Applications in Sustainable Energy and*
518 *Environmental Remediation*; Sharma, V. K., Doong, R., Kim, H., Varma, R. S.,
519 Dionysiou, D. D., Eds.; ACS Symposium Series; American Chemical Society,
520 2016; Vol. 1238, pp 161–220. <https://doi.org/10.1021/bk-2016-1238.ch007>.
- 521 (9) Sun, X. H.; Feng, M. B.; Dong, S. Y.; Qi, Y.; Sun, L.; Nesnas, N.; Sharma, V. K.
522 Removal of Sulfachloropyridazine by Ferrate(VI): Kinetics, Reaction Pathways,
523 Biodegradation, and Toxicity Evaluation. *Chem. Eng. J.* **2019**, *372*, 742–751.
524 <https://doi.org/10.1016/j.cej.2019.04.121>.
- 525 (10) Sharma, V. K.; Feng, M. B.; Dionysiou, D. D.; Zhou, H.-C.; Jinadatha, C.; Manoli,
526 K.; Smith, M. F.; Luque, R.; Ma, X. M.; Huang, C.-H. Reactive High-Valent Iron
527 Intermediates in Enhancing Treatment of Water by Ferrate. *Environ. Sci. Technol.*
528 **2022**, *56* (1), 30–47. <https://doi.org/10.1021/acs.est.1c04616>.
- 529 (11) Shao, B. B.; Dong, H. Y.; Zhou, G. M.; Ma, J.; Sharma, V. K.; Guan, X. H.
530 Degradation of Organic Contaminants by Reactive Iron/Manganese Species:
531 Progress and Challenges. *Water Res.* **2022**, *221*, 118765.
532 <https://doi.org/10.1016/j.watres.2022.118765>.
- 533 (12) Deng, Y.; Abdel-Shafy, H. I. Barriers to Ferrate(VI) Application in Water and

- 534 Wastewater Treatment. *Environ. Sci. Technol.* **2024**, *58* (7), 3057–3060.
535 <https://doi.org/10.1021/acs.est.3c09203>.
- 536 (13) Wu, Y. H.; Wang, H. Z.; Du, J. S.; Si, Q. S.; Zhao, Q.; Jia, W. R.; Wu, Q. L.; Guo,
537 W.-Q. Enhanced Oxidation of Organic Compounds by the Ferrihydrite–Ferrate
538 System: The Role of Intramolecular Electron Transfer and Intermediate Iron
539 Species. *Environ. Sci. Technol.* **2023**, *57* (43), 16662–16672.
540 <https://doi.org/10.1021/acs.est.3c05798>.
- 541 (14) Guo, B. L.; Wang, J. Y.; Sathiyar, K.; Ma, X. M.; Lichtfouse, E.; Huang, C.-H.;
542 Sharma, V. K. Enhanced Oxidation of Antibiotics by Ferrate Mediated with
543 Natural Organic Matter: Role of Phenolic Moieties. *Environ. Sci. Technol.* **2023**,
544 *57* (47), 19033–19042. <https://doi.org/10.1021/acs.est.3c03165>.
- 545 (15) Manoli, K.; Nakhla, G.; Ray, A. K.; Sharma, V. K. Oxidation of Caffeine by Acid-
546 Activated Ferrate(VI): Effect of Ions and Natural Organic Matter. *AIChE J.* **2017**,
547 *63* (11), 4998–5006. <https://doi.org/10.1002/aic.15878>.
- 548 (16) Wang, Y. P.; Xiao, Z. J.; Liu, Y. L.; Tian, W. J.; Huang, Z. S.; Zhao, X. N.; Wang,
549 L.; Wang, S. B.; Ma, J. Enhanced Ferrate(VI) Oxidation of Organic Pollutants
550 through Direct Electron Transfer. *Water Res.* **2023**, *244*, 120506.
551 <https://doi.org/10.1016/j.watres.2023.120506>.
- 552 (17) Wang, Z. J.; Yang, X.; Du, Q.; Liu, T.; Dai, X.; Du, Y.; Zhang, H.; Zhou, P.; Xiong,
553 Z. K.; Lai, B. Ferrate(VI)/Percarbonate for the Oxidation of Micropollutants:
554 Interactive Activation and Release of Low-Concentration Hydrogen Peroxide for
555 Efficient Electron Utilization. *J. Hazard. Mater.* **2024**, *469*, 134029.

- 556 <https://doi.org/10.1016/j.jhazmat.2024.134029>.
- 557 (18) Chen, X. J.; Bai, C. W.; Sun, Y. J.; Huang, X. T.; Zhang, B. B.; Zhang, Y. S.; Yang,
558 Q.; Wu, J. H.; Chen, F. pH-Driven Efficacy of the Ferrate(VI)–Peracetic Acid
559 System in Swift Sulfonamide Antibiotic Degradation: A Deep Dive into Active
560 Species Evolution and Mechanistic Insights. *Environ. Sci. Technol.* **2023**, *57* (48),
561 20206–20218. <https://doi.org/10.1021/acs.est.3c06370>.
- 562 (19) Liu, M. Z.; Wu, N. N.; Li, X. Y.; Zhang, S. N.; Sharma, V. K.; Ajarem, J. S.; Allam,
563 A. A.; Qu, R. J. Insights into Manganese(VII) Enhanced Oxidation of
564 Benzophenone-8 by Ferrate(VI): Mechanism and Transformation Products. *Water*
565 *Res.* **2023**, *238*, 120034. <https://doi.org/10.1016/j.watres.2023.120034>.
- 566 (20) Li, J.; Cao, J. C.; Jiang, M. J.; An, L. Q.; Zeng, G.; Mai, J. M.; Su, P.; Jing, B. H.;
567 Feng, M. B.; Ao, Z. M.; Ma, J.; Yang, T. Role of Bipyridyl in Enhancing Ferrate
568 Oxidation toward Micropollutants. *J. Hazard. Mater.* **2024**, *469*, 133982.
569 <https://doi.org/10.1016/j.jhazmat.2024.133982>.
- 570 (21) Chen, K. Y.; Zhu, G. M.; Huang, X. J.; Huang, X. X.; Xu, Y. M.; Pang, H. L.; Luo,
571 C. W.; Lu, J. S.; Zhang, Z. Q. New Insights into Degradation of Emerging
572 Contaminants by S(IV)/Fe(VI) System in Neutral Water: Performance
573 Enhancement, Reaction Mechanisms and Toxicity Assessment. *Sep. Purif.*
574 *Technol.* **2024**, *328*, 125112. <https://doi.org/10.1016/j.seppur.2023.125112>.
- 575 (22) Wang, Z. J.; Du, Y.; Liu, T.; Li, J.; He, C. S.; Liu, Y.; Xiong, Z. K.; Lai, B. How
576 Should We Activate Ferrate(VI)? Fe(IV) and Fe(V) Tell Different Stories about
577 Fluoroquinolone Transformation and Toxicity Changes. *Environ. Sci. Technol.*

578 **2024**, 58 (10), 4812–4823. <https://doi.org/10.1021/acs.est.3c10800>.

579 (23) Zhang, Z.; Li, X.; Zhang, C.; Lu, S. H.; Xi, Y. N.; Huang, Y. C.; Xue, Z. Z.; Yang,
580 T. Combining Ferrate(VI) with Thiosulfate to Oxidize Chloramphenicol:
581 Influencing Factors and Degradation Mechanism. *J. Environ. Chem. Eng.* **2021**, 9
582 (1), 104625. <https://doi.org/10.1016/j.jece.2020.104625>.

583 (24) Sathiyar, K.; Wang, J. Y.; Williams, L. M.; Huang, C.-H.; Sharma, V. K. Revisiting
584 the Electron Transfer Mechanisms in Ru(III)-Mediated Advanced Oxidation
585 Processes with Peroxyacids and Ferrate(VI). *Environ. Sci. Technol.* **2024**.
586 <https://doi.org/10.1021/acs.est.4c02640>.

587 (25) Tian, B. R.; Wu, N. N.; Liu, M. Z.; Wang, Z. Y.; Qu, R. J. Promoting Effect of
588 Silver Oxide Nanoparticles on the Oxidation of Bisphenol B by Ferrate(VI).
589 *Environ. Sci. Technol.* **2023**, 57 (41), 15715–15724.
590 <https://doi.org/10.1021/acs.est.3c03653>.

591 (26) Shu, J.; Xu, X. P.; Zhang, Y. C.; Wang, K. M.; Zhu, Y. X.; Lian, X. R.; Wang, H.
592 Y. Insight into the Mechanism of Ferrate(VI) Activation by Mineral Zincite for
593 Carbamazepine Degradation: Role of Fe(V) Species and Free Radical Induction.
594 *Chem. Eng. J.* **2023**, 473, 145360. <https://doi.org/10.1016/j.cej.2023.145360>.

595 (27) Yang, T.; Mai, J. M.; Cheng, H. J.; Zhu, M. Y.; Wu, S. S.; Tang, L. Y.; Liang, P.;
596 Jia, J. B.; Ma, J. UVA-LED-Assisted Activation of the Ferrate(VI) Process for
597 Enhanced Micropollutant Degradation: Important Role of Ferrate(IV) and
598 Ferrate(V). *Environ. Sci. Technol.* **2022**, 56 (2), 1221–1232.
599 <https://doi.org/10.1021/acs.est.1c03725>.

- 600 (28) Baum, J. C.; Feng, M. B.; Guo, B. L.; Huang, C.-H.; Sharma, V. K. Generation of
601 Iron(IV) in the Oxidation of Amines by Ferrate(VI): Theoretical Insight and
602 Implications in Oxidizing Pharmaceuticals. *ACS ES&T Water* **2021**, *1* (8), 1932–
603 1940. <https://doi.org/10.1021/acsestwater.1c00156>.
- 604 (29) Luo, C.; Feng, M. B.; Zhang, T. Q.; Sharma, V. K.; Huang, C.-H. Ferrate(VI)
605 Oxidation of Pharmaceuticals in Hydrolyzed Urine: Enhancement by Creatinine
606 and the Role of Fe(IV). *ACS ES&T Water* **2021**, *1* (4), 969–979.
607 <https://doi.org/10.1021/acsestwater.0c00255>.
- 608 (30) Feng, M. B.; Baum, J. C.; Nesnas, N.; Lee, Y.; Huang, C.-H.; Sharma, V. K.
609 Oxidation of Sulfonamide Antibiotics of Six-Membered Heterocyclic Moiety by
610 Ferrate(VI): Kinetics and Mechanistic Insight into SO₂ Extrusion. *Environ. Sci.*
611 *Technol.* **2019**, *53* (5), 2695–2704. <https://doi.org/10.1021/acs.est.8b06535>.
- 612 (31) Frisch, M. J.; Trucks, G. W.; Schlegel, H. B.; Scuseria, G. E.; Robb, M. A.;
613 Cheeseman, J. R.; Scalmani, G.; Barone, V.; Petersson, G. A.; Nakatsuji, H.; Li,
614 X.; Caricato, M.; Marenich, A. V.; Bloino, J.; Janesko, B. G.; Gomperts, R.;
615 Mennucci, B.; Hratchian, H. P.; Ortiz, J. V.; Izmaylov, A. F.; Sonnenberg, J. L.;
616 Williams-Young, D.; Ding, F.; Lipparini, F.; Egidi, F.; Goings, J.; Peng, B.;
617 Petrone, A.; Henderson, T.; Ranasinghe, D.; Zakrzewski, V. G.; Gao, J.; Rega, N.;
618 Zheng, G.; Liang, W.; Hada, M.; Ehara, M.; Toyota, K.; Fukuda, R.; Hasegawa, J.;
619 Ishida, M.; Nakajima, T.; Honda, Y.; Kitao, O.; Nakai, H.; Vreven, T.; Throssell,
620 K.; Montgomery, J. A.; Peralta, Jr., J. E.; Ogliaro, F.; Bearpark, M. J.; Heyd, J. J.;
621 Brothers, E. N.; Kudin, K. N.; Staroverov, V. N.; Keith, T. A.; Kobayashi, R.;

622 Normand, J.; Raghavachari, K.; Rendell, A. P.; Burant, J. C.; Iyengar, S. S.; Tomasi,
623 J.; Cossi, M.; Millam, J. M.; Klene, M.; Adamo, C.; Cammi, R.; Ochterski, J. W.;
624 Martin, R. L.; Morokuma, K.; Farkas, O.; Foresman, J. B.; Fox, D. J. Gaussian 16,
625 Revision C.01. *Gaussian Inc, Wallingford CT* **2019**.

626 (32) Becke, A. D. Density-functional Thermochemistry. III. The Role of Exact
627 Exchange. *J. Chem. Phys.* **1993**, *98* (7), 5648–5652.
628 <https://doi.org/10.1063/1.464913>.

629 (33) Lee, C.; Yang, W.; Parr, R. G. Development of the Colle-Salvetti Correlation-
630 Energy Formula into a Functional of the Electron Density. *Phys. Rev. B* **1988**, *37*
631 (2), 785–789. <https://doi.org/10.1103/PhysRevB.37.785>.

632 (34) Grimme, S.; Ehrlich, S.; Goerigk, L. Effect of the Damping Function in Dispersion
633 Corrected Density Functional Theory. *J. Comput. Chem.* **2011**, *32* (7), 1456–1465.
634 <https://doi.org/10.1002/jcc.21759>.

635 (35) Grimme, S.; Antony, J.; Ehrlich, S.; Krieg, H. A Consistent and Accurate Ab Initio
636 Parametrization of Density Functional Dispersion Correction (DFT-D) for the 94
637 Elements H-Pu. *J. Chem. Phys.* **2010**, *132* (15), 154104.
638 <https://doi.org/10.1063/1.3382344>.

639 (36) Weigend, F. Accurate Coulomb-Fitting Basis Sets for H to Rn. *Phys. Chem. Chem.*
640 *Phys.: PCCP* **2006**, *8* (9), 1057–1065. <https://doi.org/10.1039/b515623h>.

641 (37) Weigend, F.; Ahlrichs, R. Balanced Basis Sets of Split Valence, Triple Zeta
642 Valence and Quadruple Zeta Valence Quality for H to Rn: Design and Assessment
643 of Accuracy. *Phys. Chem. Chem. Phys.* **2005**, *7* (18), 3297–3305.

- 644 <https://doi.org/10.1039/B508541A>.
- 645 (38) Schäfer, A.; Huber, C.; Ahlrichs, R. Fully Optimized Contracted Gaussian Basis
646 Sets of Triple Zeta Valence Quality for Atoms Li to Kr. *J. Chem. Phys.* **1994**, *100*
647 (8), 5829–5835. <https://doi.org/10.1063/1.467146>.
- 648 (39) Schäfer, A.; Horn, H.; Ahlrichs, R. Fully Optimized Contracted Gaussian Basis
649 Sets for Atoms Li to Kr. *J. Chem. Phys.* **1992**, *97* (4), 2571–2577.
650 <https://doi.org/10.1063/1.463096>.
- 651 (40) Lu, T.; Chen, F. W. Multiwfn: A Multifunctional Wavefunction Analyzer. *J.*
652 *Comput. Chem.* **2012**, *33* (5), 580–592. <https://doi.org/10.1002/jcc.22885>.
- 653 (41) Huang, Z. S.; Wang, L.; Liu, Y. L.; Jiang, J.; Xue, M.; Xu, C. B.; Zhen, Y. F.; Wang,
654 Y. C.; Ma, J. Impact of Phosphate on Ferrate Oxidation of Organic Compounds:
655 An Underestimated Oxidant. *Environ. Sci. Technol.* **2018**, *52* (23), 13897–13907.
656 <https://doi.org/10.1021/acs.est.8b04655>.
- 657 (42) Lei, Y.; Yu, Y. F.; Lei, X.; Liang, X.; Cheng, S. S.; Ouyang, G. F.; Yang, X.
658 Assessing the Use of Probes and Quenchers for Understanding the Reactive
659 Species in Advanced Oxidation Processes. *Environ. Sci. Technol.* **2023**, *57* (13),
660 5433–5444. <https://doi.org/10.1021/acs.est.2c09338>.
- 661 (43) Li, G.; Jiang, J. C.; He, M. X.; Rao, D. D.; Zhang, J.; Sun, B. Enhancing Ferrate
662 Oxidation of Micropollutants via Inducing Fe(V)/Fe(IV) Formation Needs
663 Caution: Increased Conversion of Bromide to Bromate. *Environ. Sci. Technol.*
664 **2023**, *57* (47), 18991–18999. <https://doi.org/10.1021/acs.est.3c01395>.
- 665 (44) Guo, Y.; Zhan, J. H.; Yu, G.; Wang, Y. J. Evaluation of the Concentration and

666 Contribution of Superoxide Radical for Micropollutant Abatement during
667 Ozonation. *Water Res.* **2021**, *194*, 116927.
668 <https://doi.org/10.1016/j.watres.2021.116927>.

669 (45) Niu, L. J.; Lin, J.; Chen, W. Z.; Zhang, Q.; Yu, X.; Feng, M. B.
670 Ferrate(VI)/Periodate System: Synergistic and Rapid Oxidation of
671 Micropollutants via Periodate/Iodate-Modulated Fe(IV)/Fe(V) Intermediates.
672 *Environ. Sci. Technol.* **2023**, *57* (17), 7051–7062.
673 <https://doi.org/10.1021/acs.est.2c08965>.

674 (46) Luo, M. F.; Zhou, H. Y.; Zhou, P.; Lai, L. D.; Liu, W.; Ao, Z. M.; Yao, G.; Zhang,
675 H.; Lai, B. Insights into the Role of In-Situ and Ex-Situ Hydrogen Peroxide for
676 Enhanced Ferrate(VI) towards Oxidation of Organic Contaminants. *Water Res.*
677 **2021**, *203*, 117548. <https://doi.org/10.1016/j.watres.2021.117548>.

678 (47) Lee, H.; Lee, C.; Kim, J.-H. Response to Comment on “Activation of Persulfate
679 by Graphitized Nanodiamonds for Removal of Organic Compounds.” *Environ. Sci.*
680 *Technol.* **2017**, *51* (9), 5353–5354. <https://doi.org/10.1021/acs.est.7b01642>.

681 (48) Li, B. B.; Guo, R. X.; Tian, J.; Wang, Z. Y.; Qu, R. J. New Findings of Ferrate(VI)
682 Oxidation Mechanism from Its Degradation of Alkene Imidazole Ionic Liquids.
683 *Environ. Sci. Technol.* **2021**, *55* (17), 11733–11744.
684 <https://doi.org/10.1021/acs.est.1c03348>.

685 (49) Zong, Y.; Chen, L.; Zeng, Y. Q.; Xu, J.; Zhang, H.; Zhang, X. M.; Liu, W.; Wu, D.
686 Do We Appropriately Detect and Understand Singlet Oxygen Possibly Generated
687 in Advanced Oxidation Processes by Electron Paramagnetic Resonance

688 Spectroscopy? *Environ. Sci. Technol.* **2023**.
689 <https://doi.org/10.1021/acs.est.3c01553>.

690 (50) Zhao, L. X.; Cheng, X. Y.; Wang, Z. X.; Zhang, E. Z.; Liu, Z. L.; Zhou, H. J.; He,
691 L.; Guan, Q. Q. Generating High-Valent Iron-Oxo $\equiv\text{FeIV}=\text{O}$ Complexes by
692 Calcium Sulfite Activation in Neutral Microenvironments for Enhanced
693 Degradation of CIP. *Environ. Pollut.* **2023**, *336*, 122449.
694 <https://doi.org/10.1016/j.envpol.2023.122449>.

695 (51) Son, Y. J.; Kim, S.; Leung, V.; Kawashima, K.; Noh, J.; Kim, K.; Marquez, R. A.;
696 Carrasco-Jaim, O. A.; Smith, L. A.; Celio, H.; Milliron, D. J.; Korgel, B. A.;
697 Mullins, C. B. Effects of Electrochemical Conditioning on Nickel-Based Oxygen
698 Evolution Electrocatalysts. *ACS Catal.* **2022**, *12* (16), 10384–10399.
699 <https://doi.org/10.1021/acscatal.2c01001>.

700 (52) Narku-Tetteh, J.; Muchan, P.; Saiwan, C.; Supap, T.; Idem, R. Effect of Side Chain
701 Structure and Number of Hydroxyl Groups of Primary, Secondary and Tertiary
702 Amines on Their Post-Combustion CO₂ Capture Performance. *Energy Procedia*
703 **2017**, *114*, 1811–1827. <https://doi.org/10.1016/j.egypro.2017.03.1309>.
704